THE JOURNAL OF BIOLOGICAL CHEMISTRY VOL. 280, NO. 41, pp. 34635–34643, October 14, 2005

Functional Expression of the Human HCN3 Channel*[S]

Received for publication, March 7, 2005, and in revised form, July 18, 2005 Published, JBC Papers in Press, July 25, 2005, DOI 10.1074/jbc.M502508200

Juliane Stieber[1], **Georg Stöckl, Stefan Herrmann, Benjamin Hassfurth, and Franz Hofmann**

From the Institut für Pharmakologie und Toxikologie der Technischen Universität München, Biedersteiner Strasse 29, 80802 München, Germany

Hyperpolarization-activated, cyclic nucleotide-gated cation (HCN) channels underlie the inward pacemaker current, termed I_f/I_h, in a variety of tissues. Many details are known for the HCN subtypes 1, 2, and 4. We now successfully cloned the cDNA for HCN3 from human brain and compared the electrophysiological properties of hHCN3 to the other three HCN subtypes. Overexpression of human HCN3 channels in HEK293 cells resulted in a functional channel protein. Similar to hHCN2 channels, hHCN3 channels are activated with a rather slow time constant of 1244 ± 526 ms at −100 mV, which is a greater time constant than that of HCN1 but a smaller one than that of HCN4 channels. The membrane potential for half-maximal activation $V_{½}$ was −77 ± 5.4 mV, and the reversal potential E_{rev} was −20.5 ± 4 mV, resulting in a permeability ratio P_{Na}/P_K of 0.3. Like all other HCNs, hHCN3 was inhibited rapidly and reversibly by extracellular cesium and slowly and irreversibly by extracellular applied ZD7288. Surprisingly, the human HCN3 channel was not modulated by intracellular cAMP, a hallmark of the other known HCN channels. Sequence comparison revealed >80% homology of the transmembrane segments, the pore region, and the cyclic nucleotide binding domain of hHCN3 with the other HCN channels. The missing response to cAMP distinguishes human HCN3 from both the well cAMP responding HCN subtypes 2 and 4 and the weak responding subtype 1.

Hyperpolarization-activated, cyclic nucleotide-gated cation (HCN)[2] channels are thought to underlie the native pacemaker current, termed I_f or I_h, in the heart and brain where these channels contribute to the control of the resting membrane potential and to the rhythmic activity of excitable cells (1–4). Four mammalian genes encoding HCN channels have been identified to date (5–7). Electrophysiological studies of the three expressed HCN (HCN1, -2, and -4) channels showed (8) that each channel is activated voltage-dependent upon membrane hyperpolarization with distinct activation kinetics (5, 9, 10). Activation of the HCN channels is directly modulated by cyclic nucleotides (11). However, the modulatory effect depends on the subtype (12, 13); activation of HCN2 and HCN4 is accelerated much more by cAMP than that of HCN1 channels. Similarly, cAMP shifts the membrane potential for activation to a larger extent for HCN2 and HCN4 than for HCN1. cAMP modulation is mediated by direct binding of cAMP to a cyclic nucleotide binding domain (CNBD) located in the intracellular C terminus, thereby releasing the inhibitory effect of this C terminus on channel activation (13–15).

The functional expression of HCN3 channels proved to be difficult. Expression of the murine HCN3 in HEK293 cells or similar systems resulted in very small and unstable currents. Only recently, expression of the murine HCN3 channel was improved by using a lentiviral-based approach (16). Thus, information about the basic biophysical and pharmacological properties of HCN3 channels, in comparison to the other HCN channels, is limited (5, 8, 16, 17). Especially, the modulation by cyclic nucleotides is still under investigation. We now cloned the HCN3 channel from human brain. Stable expression of hHCN3 in HEK293 cells allowed a more detailed characterization of this HCN channel and comparison to the other three human HCN subtypes. hHCN3/hHCN4 chimeric channels contributed to the understanding of how cAMP modulates HCN channels.

EXPERIMENTAL PROCEDURES

Cloning of cDNAs Coding for HCN Channels—Human HCN3 cDNA was cloned from whole human brain QUICK-Clone cDNA (Clontech) using an overlapping PCR strategy. Two cDNA fragments were amplified using the primer pairs hHCN3f1 (5′-CTAGGAGGCCGAGCGTGTAAGCGGGGT-3′)/hHCN3r1 (5′-AGTCCCTGGACTCTTCCCGGCGTCAGT-3′) and hHCN3f2 (5′-GCCACGGCACTCATCCAGTCCCTGGAC-3′)/hHCN3r2 (5′-AACATGTAAAACCTTTGAGTACATCCA-3′). The two fragments with 1.1 and 1.3 kilobases, respectively, were ligated via the PflMI restriction site and cloned into the pcDNA3 mammalian expression vector (Invitrogen). The human HCN1 cDNA was cloned from the same source. The sequences of the primer pairs were hHCN1f1 (5′-GGGCATGGAAGGAGGCGGCAA-3′)/hHCN1r1 (5′-AGGCGGCAGTATCAAGAGAAG-3′) and hHCN-1f2 (5′-CACCTGCTATGCCATGTTTGT-3′)/hHCN1r2 (5′-TTGTCAAAGCAGAAAGAAATAC-3′). The two fragments, with 1.2 and 1.5 kilobases, respectively, were ligated via the PflMI restriction site and cloned into the pcDNA3 vector. The identity of hHCN1 and hHCN3 clones was verified by DNA sequencing and comparing the sequence to the sequences accessible in the human genome data base (for accession numbers, see Supplement Table S1). Human HCN2 and HCN4 cDNAs were originally cloned from the atrioventricular node region of a human heart (9) and subcloned into the pcDNA3 vector. Murine HCN3 cDNA was originally cloned from mouse brain (7).

Establishment of Stable hHCN Cell Lines—All four hHCN plasmids (cDNA in vector pcDNA3, containing a neomycin open reading frame) were linearized using the unique restriction site PvuI located in the ampicillin open reading frame of the vector. Transfection of HEK293 cells was performed separately with each linearized HCN construct via electroporation (Bio-Rad electroporation system) following the manufacturer's instructions. 48 h after transfection 0.4 mg/ml G418 (neomycin) was added to the cell medium for selection. After 3 weeks in selection medium, resistant cell clones were picked and checked for RNA transcription by Northern blotting, protein expression by Western blotting, and the presence of HCN currents by patch clamp recordings. HCN-expressing cells were cultured in complete medium (Quantum286, PAA) with 0.2 mg/ml G418 at 37 °C, 8.5% CO_2. For longer

* This research was supported by grants from Deutsche Forschungsgemeinschaft and Fonds der Chemie. The costs of publication of this article were defrayed in part by the payment of page charges. This article must therefore be hereby marked "*advertisement*" in accordance with 18 U.S.C. Section 1734 solely to indicate this fact.

[S] The on-line version of this article (available at http://www.jbc.org) contains supplemental Figs. S1–S3 and Tables S1 and S2.

[1] To whom correspondence should be addressed. Tel.: 49-89-4140-3286; Fax: 49-89-4140-3261; E mail: stieber@ipt.med.tu-muenchen.de.

[2] The abbreviations used are: HCN, hyperpolarization-activated, cyclic nucleotide-gated cation channel; hHCN, human HCN; HEK, human embryonic kidney cells; CNBD, cyclic nucleotide binding domain; pCPT-cGMP, 8-(4-Chlorophenylthio)-guanosine 3′,5′-cyclic monophosphate.

storage, cells in complete medium with 4% Me_2SO are kept in liquid nitrogen.

Construction of hHCN3/hHCN4 Chimeric Channel Mutants and Transient Expression in HEK293 Cells—hHCN3/4 chimeric channel mutants were constructed in the pcDNA3 mammalian expression vector (Invitrogen) using overlapping PCR strategies. Briefly, DNA fragments containing the desired sequences were generated in several PCR steps using the hHCN3 and hHCN4 wild type cDNAs as templates and cloned into the HindIII/XbaI sites of the pcDNA3 vector. The correctness of the mutant channels was verified by DNA sequencing. HEK293 cells were transiently transfected with the mutant HCN channels using FuGENE 6 transfection reagent (Roche Applied Science) according to the manufacturer's instructions (transfectant/DNA ratio: 3/1 v/w). Cells were cultured in minimum Eagle's medium supplemented with 10% fetal calf serum and kept at 37 °C, 6% CO_2. Currents were recorded 2–3 days after transfection as described under "Electrophysiology" (this section of text).

Dot Blot Analysis—Dot blot analysis was performed using a human multiple-tissue expression array (BD Biosciences Clontech) containing normalized loadings of poly(A)$^+$ RNA from different human tissues. PCR fragments of hHCN1–4, amplified using the following oligonucleotides, were used as templates for the generation of ^{32}P-labeled cDNA probes by random primed labeling (Random Primed DNA labeling Kit, Roche Applied Science): hHCN1, 5′-TGTCATTCAGGATCCACCCTGAATTCCACATCGTC (forward) and 5′-GCTTGAACTGGTACCCTGCTGTTGCATGAGTGACA (reverse); hHCN2, 5′-TACTTAGATGGATCCAGCTTCATGCAGCGCCAGTT (forward) and 5′-GTATCAATAGGTACCTCCTTGAAGAAGGTGATGCC (reverse); hHCN3, 5′-TGGATCCTAGGATCCTATTGTCTGATACTTTCTTCC (forward) and 5′-AAATGGCGCGTGGTACCGCGTCCAACCGTGGCTCCAG (reverse); hHCN4, 5′-AATCAGACTGGATCCCAGTGGGAGCAGCGGGGGCC (forward) and 5′-GAATTGGCTGGTACCTGGCAGTTTGGAGCGCACTG (reverse). Hybridization and washing conditions for the blots followed the manufacturer's instructions, with a prehybridization step of 30 min and an overnight hybridization step (all at 65 °C). The hybridized probe was visualized using BAS-1500 phosphorimaging (Fuji) after a total exposure time of 48 h.

Northern Blot Analysis—Total RNA was isolated from HEK293 cells transfected with of hHCN1, hHCN2, hHCN3, or hHCN4 using RNA blood mini kit (Qiagen). 2 μg of total RNA per lane were separated on a 0.9% formaldehyde gel for 4 h at 4 °C. Blotting and hybridization with the HCN probes (see above) were carried out overnight. After two washing steps, the hybridized probe was visualized with phosphorimaging after an exposure time of 24 h. The same blot was probed subsequently with the four HCN probes. The blot was stripped between each hybridization with SDS-containing buffer. To estimate the sizes of the RNA bands, a RNA ladder (New England Biolabs) containing fragments from 0.5 to 9 kilobases was used.

Western Blot Analysis—Western blot analysis of HCN- or mock-transfected HEK293 cells with specific antibodies against HCN1, -2, -3, and -4 was performed basically as described (9, 18). Specific antibodies against HCN1 and HCN2 were obtained from Alomone Labs (Israel), HCN3-specific antibody was raised against the 228 amino acids (amino acids 552–779) after the end of the CNBD of the murine HCN3, and HCN4-specific antibody was raised against a peptide (TAAPQREPGARSEPVRSK) from the C terminus of the murine HCN4 as described in Stieber *et al.* (18). Lysates from HEK293 cells (5–10 μg of total protein per lane) were applied on a 7.5% SDS-PAGE gel, separated, blotted, and probed with the antibodies using a chemiluminescence detection system.

Electrophysiology—Electrophysiological recordings were performed as described (13). Currents were recorded in whole cell configuration at 23 ± 1 °C using a MultiClamp 700A amplifier and pClamp9 software (Axon Instruments/Molecular Devices). Analysis was done offline with Origin 6.0 software (Microcal). Borosilicate glass pipettes for recording had a resistance of 2–5 megaohms when filled with intracellular (pipette) solution which contained 10 mM NaCl, 30 mM KCl, 90 mM potassium aspartate, 1 mM $MgSO_4$, 3 mM Mg-ATP, 5 mM EGTA, and 10 mM HEPES, pH adjusted to 7.4 with KOH. The extracellular (bath) solution contained 120 mM NaCl, 20 mM KCl, 1 mM $MgCl_2$, 1.8 mM $CaCl_2$, 10 mM HEPES, and 10 mM glucose, pH adjusted to 7.4 with NaOH. The membrane potential was held at −40 mV. To elicit inward currents, step pulses of various durations were applied from −140 to −30 mV followed by a step to −140 mV (Fig. 2*B*). To account for the different activation kinetics, the duration of the prepulses were, if not stated otherwise: hHCN1, 0.5 s; hHCN2 and hHCN3, 3s; hHCN4, 8s. Time constants of activation (τ_{act}) were obtained by fitting the current traces of the −140 to −90 mV steps after the initial lag with the sum of two exponential functions:

$$y_0 + A_1 e^{\frac{x}{\tau_1}} + A_2 e^{\frac{x}{\tau_2}} \qquad \text{(Eq. 1)}$$

where τ_1 and τ_2 are the fast and slow time constants of activation, respectively; τ_1 is consequently referred to as τ_{act} since the slow component (A_2) generally accounts for <20% of the current amplitude. To obtain voltage-dependent steady-state activation curves, tail currents measured immediately after the final step to −140 mV were normalized by the maximal current (I_{max}) and plotted as a function of the preceding membrane potential. The curves were fitted with the Boltzmann function,

$$\frac{I - I_{min}}{I_{max} - I_{min}} = \frac{A_1 - A_2}{1 + e^{\frac{V - V_{1/2}}{k}}} + A_2 \qquad \text{(Eq. 2)}$$

where I_{min} is an offset caused by a nonzero holding current and is not included in the current amplitude, V is the test potential, $V_{½}$ is the midpoint of activation, and k is the slope factor. For determination of the reversal potential (E_{rev}), channels were maximally activated by a pulse to −130 mV for 2–10 s (depending on channel subtype), then test pulses from −100 mV to +40 mV were applied. E_{rev} is the potential at which the ion flow changes from the inward to the outward direction. To get the current density, the amplitude was divided by the cell capacitance, obtained by the capacitance compensation function of the amplifier. The permeability ratio P_{Na}/P_K was calculated using the Goldman-Hodgkin-Katz voltage equation,

$$E_{rev} = -\frac{2.3RT}{F} \log\left(\frac{[K]_{in} + P_R \times [Na]_{in}}{[K]_{out} + P_R \times [Na]_{out}}\right) \qquad \text{(Eq. 3)}$$

where $P_R = P_{Na}/P_K$ and $2.3RT/F = 59.17$ at 25 °C. The effect of cAMP or cGMP was tested by recording the basic parameters before and after switching to a bath solution containing 100 μM 8-Br-cAMP or 100 μM pCPT-cGMP (both Sigma). The effect of cesium was tested by repeatedly activating HCN channels by stepping from −40 to −100 mV. After 5–10 activations, superfusion was switched to a bath solution containing Cs^+; after another 5–10 activations, superfusion was switched back to the normal bath solution. The effect of ZD7288 was tested by repeatedly activating HCN channels by stepping from −40 mV to −100 mV.

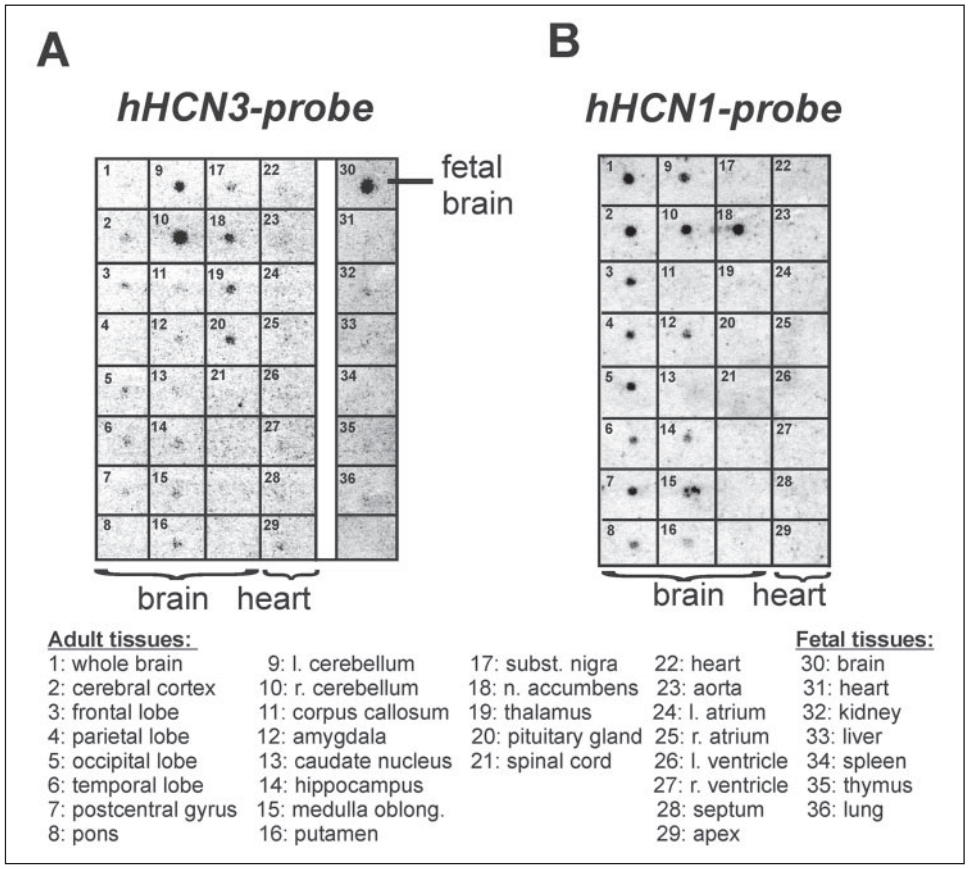

FIGURE 1. **HCN expression in human tissues.** *A*, human mRNA dot blot, probed for HCN3, demonstrates expression of HCN3 in a variety of brain tissues including a high level expression in fetal brain but in no other tissues (particularly not in cardiac tissues). *B*, the same blot as in *A* was stripped and re-probed for HCN1. Similar to HCN3, HCN1 expression is restricted to brain tissues but generally on a higher level. No expression of HCN1 could be detected in human fetal brain.

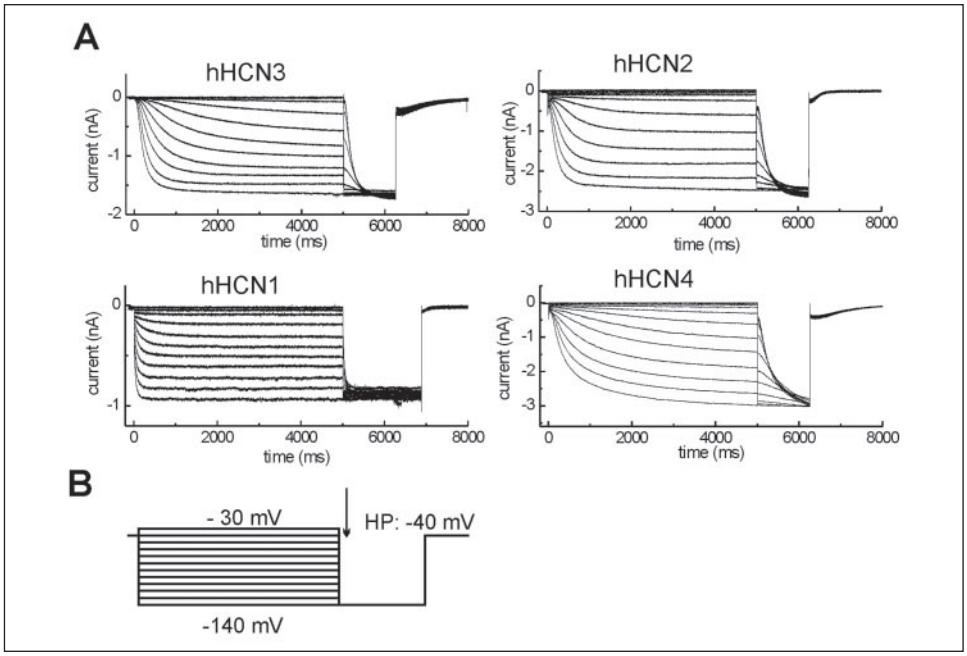

FIGURE 2. **Electrophysiological recordings of hHCN channels expressed in HEK293 cells.** *A*, representative current traces of HEK293 cells expressing one of the four HCN channels. Note that all currents are recorded with the same time scale. The pulse protocol as shown in *B* was used. The first step, an activation for 500 ms to 5 s (depending on the HCN subtype) at potentials between −140 and −30 mV were used to determine voltage-dependent activation time constants. The second step, a pulse to −140 mV after the initial activations at various potentials (*arrow*), was used to determine the voltage-dependent activation curves and the midpoint of activation ($V_{1/2}$). *HP*, holding potential.

After 8–10 activations, superfusion was switched to a bath solution containing ZD7288. A steady-state block was reached after 3–4 min. The blocking effect was calculated as residual current relative to maximal current before application of the substances. For the dose-response curves, increasing doses of cesium or ZD7288 starting at 0.01 μM were added to the bath. All values are given as the mean ± S.D.; n is the number of experiments. Statistical differences were determined using Student's unpaired t test; p values <0.05 were considered significant.

RESULTS

Low Overall Expression of HCN3 in Human Brain—Human HCN3 mRNA could be detected by dot blot analysis only in neuronal tissues.

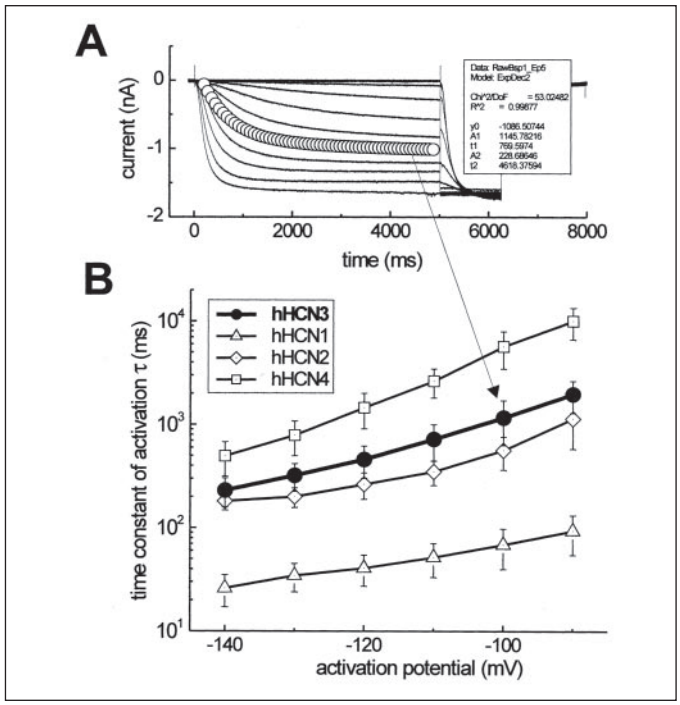

FIGURE 3. **Activation kinetics of hHCN channels.** *A*, the exponential fit (*open circles*), described under "Experimental Procedures," used to determine time constants of activation is exemplary displayed upon the current trace elicited at −100 mV from a hHCN3-transfected HEK293 cell (the same current trace as in Fig. 2*A*). In this example, τ_1 was calculated as 770 ms. *B*, voltage-dependent activation time constants for hHCN1–4 channels. Note the logarithmic scale of τ. All values are the mean ± S.D.; $n = 12–20$ cells per experiment. *Filled circles/bold line*, hHCN3; *open triangles*, hHCN1; *open diamonds*, hHCN2; *open squares*, hHCN4.

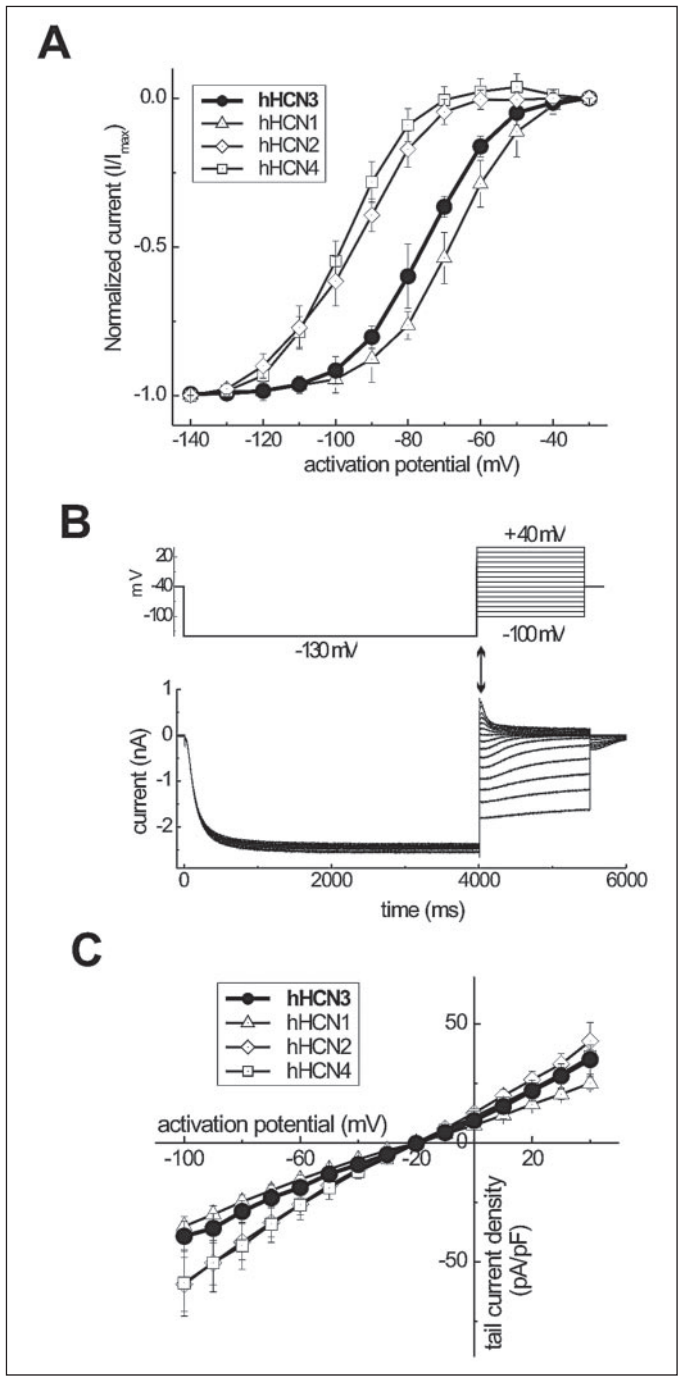

FIGURE 4. **Voltage-dependent activation and current/voltage relation of hHCN channels.** *A*, normalized voltage-dependent activation curves for hHCN1–4 channels from which $V_{1/2}$ is calculated. *B*, *upper panel*, pulse protocol applied to determine the reversal potential E_{rev}. *B*, *lower panel*, representative hHCN3 current trace. The tail current amplitudes elicited immediately after the step to the test voltages (*arrow*) were used to determine E_{rev}. *C*, current/voltage relation of the 4 hHCN channels. E_{rev} is at ~−20 mV for all 4 HCN channels. In the fully activated state, no inward or outward rectification could be detected for any of the HCN channels. All values are the mean ± S.D.; $n = 12–20$ cells per experiment. *Filled circles/bold line*, hHCN3; *open triangles*, hHCN1; *open diamonds*, hHCN2; *open squares*, hHCN4. *pF*, picofarads.

The highest expression level was found in fetal brain (Fig. 1*A*). The overall expression level was relatively low compared with the expression of human HCN1 mRNA in brain tissues (Fig. 1*B*). hHCN1 mRNA was not detected in human fetal brain. Because HCN1 and HCN3 are potential pacemaker channels, expression in cardiac tissues was also expected, as has been described at least for HCN1 in other species (19, 20) and recently for HCN3 in mouse heart (16). However, neither HCN1 nor HCN3 mRNAs could be detected in human heart. Probing a human tissue Northern blot for HCN1 and HCN3, as has been done in Ludwig *et al.* (9) for HCN2 and HCN4, confirmed that only HCN2 and HCN4 mRNAs are transcribed in human heart at detectable levels (data not shown).

Functional Expression of Human HCN Channels in HEK293 Cells—Transient, high level expression of HCN channels in HEK293 cells led to very variable current densities and, especially for HCN3 and HCN4, to enhanced cell death. Thus, we established stable HEK293 cell lines for each of the 4 HCN channels by undirected integration of the HCN coding sequence into the genome of the host cell. Northern blot (Supplemental Fig. S1*A*) and Western blot analysis (supplemental Fig. S1, *B* and *C*) of HCN-expressing HEK293 cells confirmed the expression of the correct HCN subtype at easily detectable levels. Interestingly, HEK293 cells transfected with the murine HCN3 cDNA showed protein expression at an equally high level as human HCN3 transfected cells (supplemental Fig. S1*B*) even though murine HCN3 currents were generally very small and unstable (data not shown).

We obtained cell lines with both high and low expression of human HCN protein and resulting large and small HCN current densities. For electrophysiological evaluation, cell clones were chosen with current densities of ~20–100 picoamperes/picofarads at −140 mV. This corresponds to current amplitudes of 1–3 nA and cell sizes, represented by capacitance, of 10–50 picofarads. Fig. 2*A* shows examples of typical whole cell HCN currents of the indicated subtype, recorded with the protocol displayed in Fig. 2*B*. All four hHCN clones induce stable voltage-dependent inward cation currents with distinct activation kinetics. Supplemental Fig. S2 confirms

TABLE ONE

Electrophysiological properties of hHCN channels, expressed in HEK293 cells

$V_{1/2}$, midpoint of activation; slope factor; k from the Boltzman function used to fit the voltage-dependent activation curve; τ_{-100}, time constant of activation at −100 mV; E_{rev}, reversal potential in 20 mM extracellular potassium. Values are the mean ± S.D. for 12–20 cells per channel and condition (−cAMP and +cAMP in the bath solution).

	Unmodulated				cAMP-modulated			
	$V_{1/2}$	Slope factor	τ_{-100mV}	E_{rev}	$V_{1/2}$	Slope factor	τ_{-100mV}	E_{rev}
	mV		*ms*	*mV*	*mV*		*ms*	*mV*
hHCN1:	−69.5 ± 3.3	8.9 ± 1.8	67 ± 16	−20.7 ± 5.5	−63.3 ± 7.3	8.2 ± 0.9	48 ± 13	−26.5 ± 6.4
hHCN2:	−95.6 ± 3.8	10.9 ± 1.1	562 ± 198	−19.1 ± 5.2	−67.1 ± 6.2	7.8 ± 1.7	270 ± 81	−20.0 ± 4.4
hHCN3:	−77.0 ± 5.3	9.6 ± 1.8	1244 ± 526	−20.5 ± 4.5	−79.9 ± 3.1	8.6 ± 1.3	1390 ± 312	−22.7 ± 4.3
hHCN4:	−100.5 ± 3.3	9.0 ± 2.5	5686 ± 2234	−20.1 ± 4.8	−77.5 ± 5.7	9.4 ± 1.1	1448 ± 659	−24.7 ± 9.3

that non-transfected wild type HEK293 cells do not show any inward currents when the protocol of Fig. 2*B* (or Fig. 4*B*) is applied.

Human HCN3 Channels Have, Compared with the Other HCN Subtypes, an Intermediate Activation Kinetic and I-V-relation but the Same Reversal Potential—The voltage dependence of the activation time constants is shown in Fig. 3. In the activation potential range from −140 to −90 mV, hHCN2 and hHCN3 have similar activation kinetics, whereas HCN1 is much faster, and HCN4 is much slower activated. However, even the relatively small difference between HCN2 and HCN3 is statistically significant at $p < 0.005$. These curves clearly show that hHCN1 is faster than (<) hHCN2 < hHCN3 < hHCN4 at all voltages. Comparison of voltage-dependent activation curves and the midpoint of activation $V_{½}$ (Fig. 4*A* and TABLE ONE) reveals that hHCN3 channels are activated at significantly more positive potentials than both hHCN2 and hHCN4 (differences between HCN2 and 4 are not significant) but at slightly more negative potentials than hHCN1. The difference between HCN1 and HCN3 is significant at $p < 0.001$. The reversal potential E_{rev} has been determined for all four hHCN channels using the protocol displayed in Fig. 4*B*. The cation flow through the opened channels reverses at about −20 mV in 20 mM extracellular K^+ for all hHCN channels. HCN3 does not differ in this respect. Calculation of the permeability ratio P_{Na}/P_K using the Goldman-Hodgkin-Katz voltage equation confirms that HCN3, like the other HCN channels, conduct both potassium and sodium ions with an about 3:1 preference for potassium ions. For a summary of the basic electrophysiological properties, please refer to TABLE ONE.

Human HCN3 Channels Are Rapidly and Reversibly Blocked by Extracellular Cesium Ions—It has been described some time ago (7, 21, 22) that native I_f and cloned HCN channels underlying I_f are blocked by extracellularly applied cesium. In that respect, human HCN3 is not different from any of the other subtypes (Fig. 5, *A–C*). Fig. 5*A* displays an example recorded from a hHCN3-expressing cell that is repeatedly activated with steps to −100 mV. Switching from a normal bath solution to a bath solution containing 2 mM cesium rapidly blocked the HCN current. The release of block was equally rapid upon switching back to bath solution without cesium. All 4 hHCN channels are rapidly, within 10 s, blocked by cesium (Fig. 5*B*). The dose-response curves for all hHCN channels (Fig. 5*C*) reveal similar affinities for cesium, with IC_{50} values of 201 ± 19, 206 ± 30, 157 ± 16, and 175 ± 20 μM for hHCN1, -2, -3, and -4, respectively. None of the differences are significant.

Human HCN3 Channels Are Blocked by the Specific I_f Blocker ZD7288—Among other substances, ZD7288 has been identified as a relative specific blocker of the native I_f current in sino-atrial node cells (23). ZD7288 has also been shown to block, for example, cloned and heterologously expressed HCN1 channels (24). We now found that ZD7288 indeed blocks all HCN channel subtypes, including hHCN3 (Fig. 5, *D–F*). Application of ZD7288 to the bath solution results in the inhibition of current flow. The onset of action is relatively slow; it takes 3–4 min until the steady-state inhibition is reached (Fig. 5*E*). This may be due to the fact that ZD7288 does not easily cross the cell membrane because application of ZD7288 on HCN channels from the inside of the cell membrane in inside-out patch mode (24) results in a fast inhibition of the current flow, within seconds. The inability to release the block by (extracellular) washout may confirm the fact that ZD7288 cannot cross the cell membrane to get out of the cell especially since washout in the inside-out patch mode is possible (24). The dose-response curves of all four hHCN channels (Fig. 5*F*) show no significant differences in the affinity for ZD7288, with IC_{50} values of 20 ± 6, 41 ± 15, 34 ± 11, and 21 ± 14 μM for hHCN1, -2, -3, and -4, respectively. These values are similar to the IC_{50} for mHCN1 reported in Shin *et al.* (24). The results with ZD7288 and cesium suggest that hHCN3 is a "typical" HCN channel despite the lack of response to cyclic nucleotide monophosphates described below.

Human HCN3 Channels Are Not Modulated by Intracellular cAMP or cGMP—The addition of 100 μM concentrations of the membrane-permeable cAMP analog 8-Br-cAMP to the bath solution results in a modulation of the voltage-dependent activation and activation kinetics of hHCN1, -2, and -4 but not hHCN3 (Fig. 6 and TABLE ONE). In agreement with previous observations (13), hHCN2 and hHCN4 are well modulated by cAMP; the midpoint of activation $V_{½}$ is shifted by 28.5 ± 5.9 and 23 ± 8.1 mV, respectively, toward more positive activation potentials (Fig. 6, *A* and *B*). Furthermore, activation of hHCN2 and hHCN4 channels was accelerated 2.2- and 4-fold, respectively (Fig. 6, *C* and *D*). hHCN1 is also modulated by cAMP, albeit to a lesser extent; the rightward shift of the activation curve is only 6.7 ± 4.0 mV, the acceleration of activation 1.4-fold. Both effects, however, are statistically significant at $p < 0.05$ *versus* the unmodulated state. The addition of 100 μM concentrations of the membrane-permeable cGMP analog pCPT-cGMP to the bath solution also results in a positive modulation of hHCN1, -2, and -4 (Fig. 6*A*). The modulation is less than for 100 μM cAMP, with shifts of $V_{½}$ toward more positive activation potentials by 3.9 ± 2.1 mV (hHCN1, not significant), 13.1 ± 5.1 (hHCN2, significant), and 13.4 ± 1.6 (hHCN4, significant). Time constants of activation (Fig. 6*C*), however, are even less modulated by cGMP; activation kinetics of hHCN1, -2, and -4 are all slightly accelerated, but the difference is only significant with hHCN2.

Human HCN3 channels, on the other hand, neither show a positive reaction to cAMP nor cGMP; $V_{½}$ even shifts by 3.6 ± 4.3 mV (cAMP) and 1.6 ± 5.8 mV (cGMP) to slightly more negative potentials. This, however, indicates rundown rather than a negative modulation by cAMP/cGMP. Rundown was observed with all hHCN channels when measured without cAMP for a longer period of time. For example, a shift of $V_{½}$ by 2–8 mV to more negative potentials after 10 min superfusion with 0 μM cAMP (bath solution) was determined for hHCN1, -2, -3, and

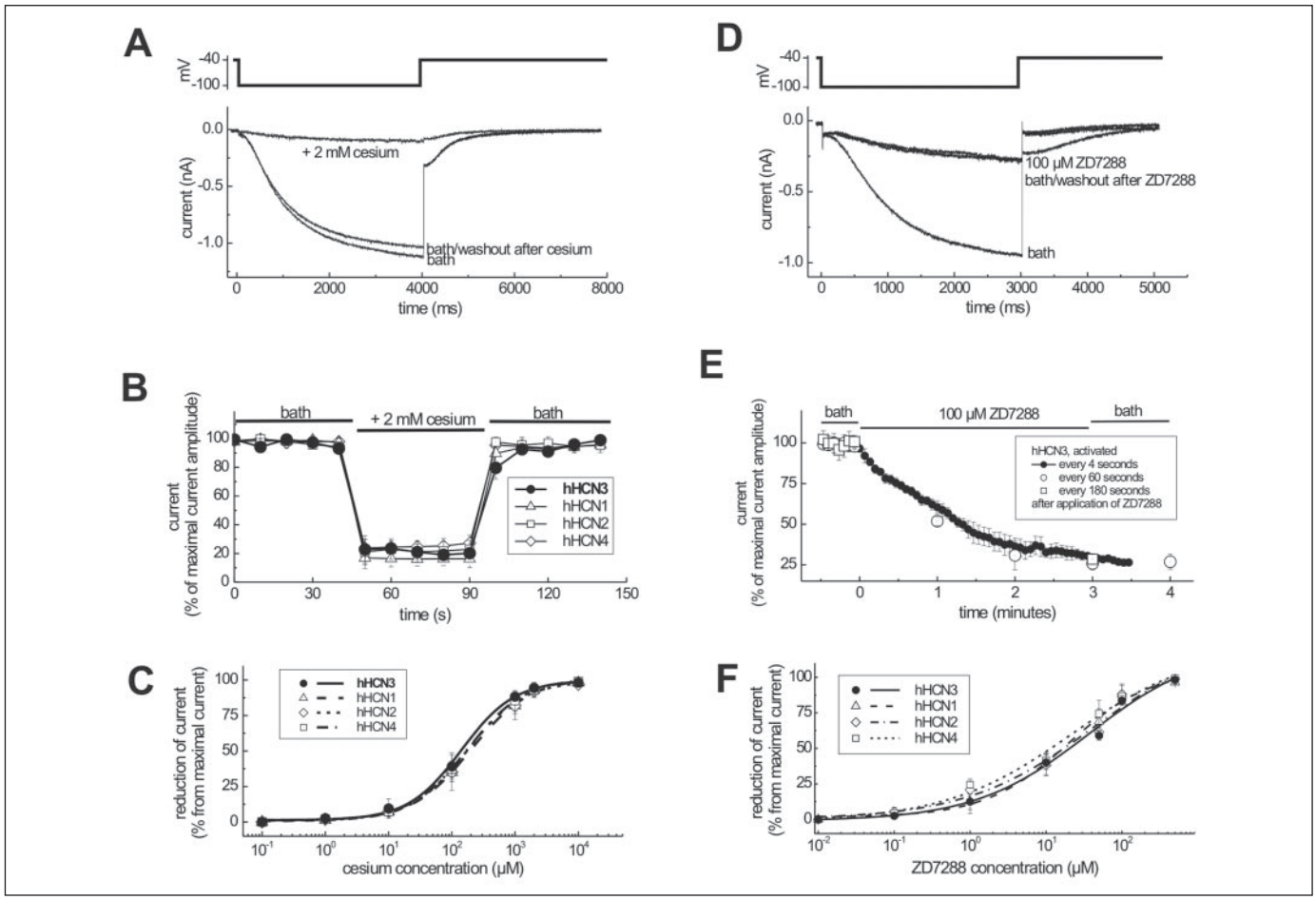

FIGURE 5. **Inhibition of HCN current by cesium and ZD7288.** *A* and *D*, *upper panels*, pulse protocols. Cells were held at a holding potential of −40 mV. HCN currents were repeatedly activated by steps to −100 mV. *A*, *lower panel*, representative current traces from a HEK293 cell expressing hHCN3. Displayed is the current trace after 4 activations in normal bath solution (*bath*); the trace 20 s after superfusion has been changed to bath solution containing 2 mM cesium (*+2 mM cesium*), and the trace 20 s after superfusion has been changed back to normal bath solution (*bath/washout after cesium*). *B*, HCN currents inhibited by 2 mM cesium. Values are the means ± S.D. of the current from 8 cells/channel during superfusion with bath and bath solution containing 2 mM cesium, normalized to the maximal current measured in bath solution. All four hHCN channels are rapidly blocked by cesium, and the block is rapidly released when cesium is washed out. *C*, dose-response curves for the Cs^+ block of hHCN channels. *Symbols* represent means of current reduction at each concentration, and *lines* represent a Boltzmann fit from which the IC_{50} was determined. The IC_{50} values for the block do not differ significantly between the four HCN subtypes, *D*, *lower panel*, representative current traces from a HEK293 cell expressing hHCN3. Displayed is the current trace after 4 activations in normal bath solution (*bath*); the current trace 3 min after superfusion has been changed to bath solution containing 100 µM ZD7288, and the current trace 1 min after superfusion has been changed back to normal bath solution (*bath/washout after ZD7288*). *E*, time-dependent inhibition of HCN currents by 100 µM ZD7288. Extracellularly applied ZD7288 inhibits HCN currents slowly and irreversible. The development of the block does not depend on repeated activation of the channel since slower activation frequencies (*open circles*, activation every minute; *open squares*, first activation after ZD7288 application after 3 min) results in the same degree of inhibition. *F*, dose-response curves for ZD7288 block of hHCN channels. *Symbols* represent means of current reduction at each concentration, and *lines* represent Boltzmann fit from which the IC_{50} was determined. The IC_{50} values for the block do not differ significantly between the four HCN subtypes.

-4 (data not shown). The difference between the negative shift observed with hHCN3 after cAMP application and the shift observed in the control experiments was not significantly different. Similar to the shift in $V_{½}$, the mean activation time constant at −100 mV is slightly increased for hHCN3 channels, indicating *deceleration* of activation as a sign of rundown and missing cAMP modulation. To rule out the possibility that the used cAMP solutions were inactivated and, thus, no effect on hHCN3 was observed, measurements were always done with hHCN3 and at least one of the other HCN channels alternately using the same solutions.

In the Core Region, Human HCN3 Channels Are Considerably Homologous to the Other Three Human HCN Channels—Human HCN3 is the smallest of all human HCN proteins with only 774 amino acids (aa), compared with 889 aa (hHCN1 and hHCN2) and 1203 aa (hHCN4) (Supplemental Table S1). The differences in length are almost exclusively due to the different lengths of the N termini proximal of the first transmembrane segment and the C termini distal from the CNBD. The N and C termini of hHCN3 are 88 and 220 amino acids, respectively, compared *e.g.* to 257 and 481 amino acids of hHCN4, the longest of the HCN proteins. The overall homology of hHCN3 with the other hHCNs is between 46 and 56% (please refer to Supplemental Table S2 for all homology data). Again, the differences are primarily due to the low homology of the N and C termini. The core region, which includes the six transmembrane segments, S1-S6, the pore region between S5 and S6, the C-linker, and the CNBD share a high similarity of up to 100% among all HCN channels. The sequence alignment of the core region of the four HCNs is shown in Supplemental Fig. S3. Differences in the electrophysiological properties including the differential reaction to cAMP are obviously not due to major amino acid deviations in the core region.

Despite the Lack of Functional Response, the CNBD of hHCN3 Channels Can Bind cAMP—The lack of a functional response to cyclic nucleotides despite the presence of a CNBD raises the question of whether the lack of response may be simply due to the fact that the CNBD cannot bind cyclic nucleotides. The CNBDs of hHCN3 and hHCN4, for example, differ by 22 of 120 amino acids from each other. This difference

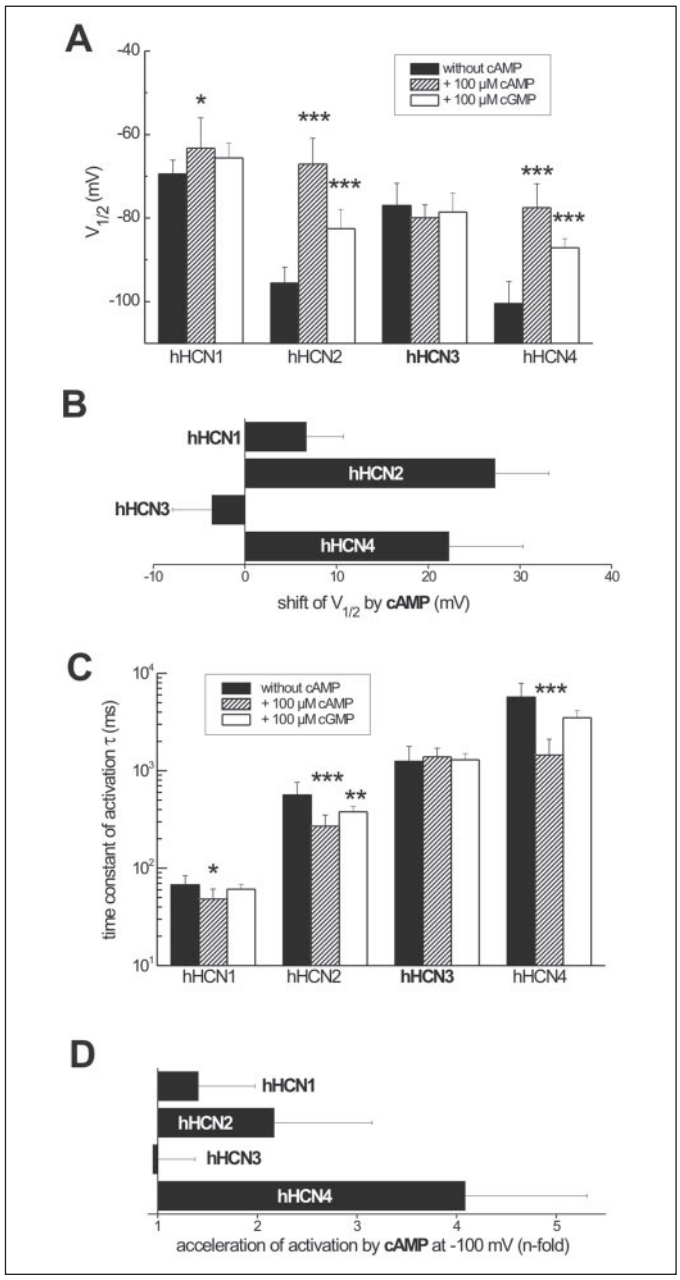

FIGURE 6. **cAMP and cGMP modulation of hHCN channels.** *A*, $V_{1/2}$ for all HCN channels after application of 100 μM 8-Br-cAMP (*striated columns*) or 100 μM pCPT-cGMP (*white columns*) to the bath solution, compared with $V_{1/2}$ before application of the cyclic nucleotide monophosphates (*black columns*). *B*, shift of $V_{1/2}$ by cAMP, calculated from *A*. *C*, time constants of activation (τ) at −100 mV for all hHCN channels before (*black columns*) and after (*striated/white columns*) application of 100 μM 8-Br-cAMP/100 μM pCPT-cGMP to the bath solution. *D*, acceleration of HCN channel activation at −100 mV by cAMP, calculated from *C*. Values are the mean ± S.D.; n = 12–20 cells per experiment. ***, $p < 0.0001$; **, $p < 0.01$; *, $p < 0.05$ (modulated *versus* unmodulated) in *A* and *C*.

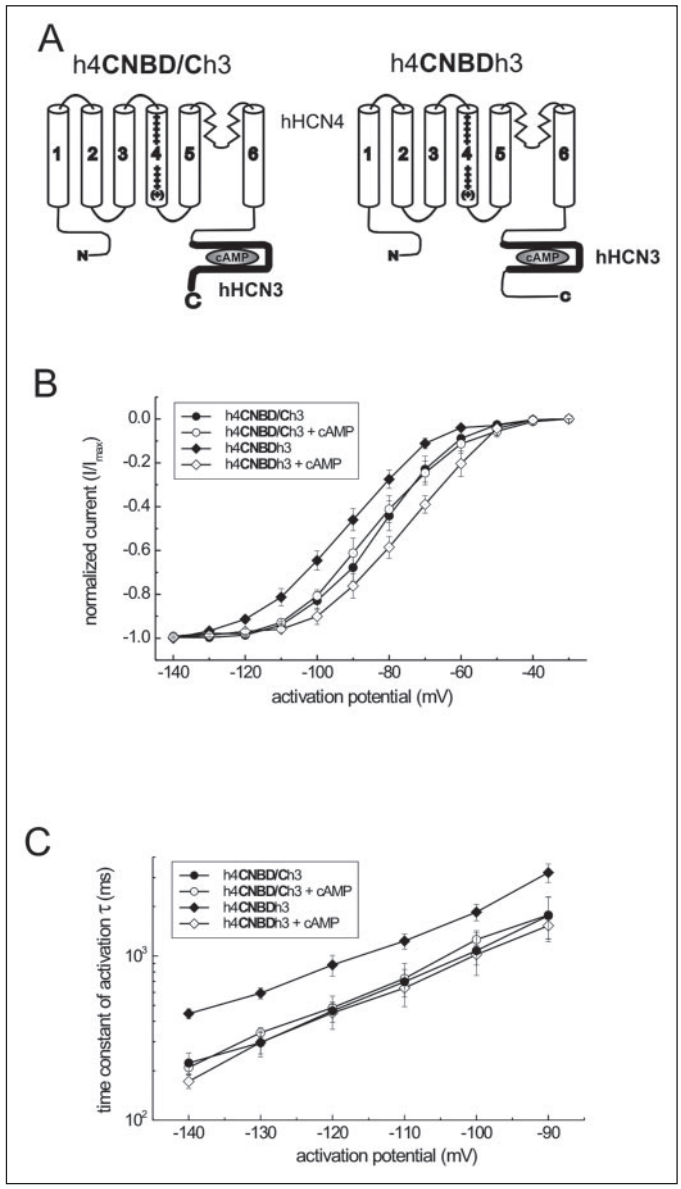

FIGURE 7. **cAMP modulation of hHCN3/hHCN4 chimeric channel mutants.** *A*, schematic representation of the two chimeric mutant HCN channels used to demonstrate the integrity of the hHCN3-CNBD. Shown are normalized voltage-dependent activation curves (*B*) and voltage-dependent activation time constants (*C*) for the two mutant channels. Symbols in *B* and *C*: *closed circles*, h4**CNBD/C**h3; *open circles*, h4**CNBD/C**h3 after application of 100 μM 8-Br-cAMP; *closed diamonds*, h4**CNBD**h3; *open diamonds*, h4**CNBD**h3 after application of 100 μM 8-Br-cAMP. The exchange of the CNBD results in a functional, HCN4-like channel that is modulated (shift to more positive activation potentials and acceleration of activation) by cAMP. cAMP modulation, however, is missing when in addition to the CNBD the rest of the C terminus is also derived from hHCN3. In the voltage-dependent activation, this chimera resembles hHCN3 wild type.

could of course influence the cAMP affinity. To clarify this question, two hHCN3/hHCN4 chimeric mutant channels were constructed (Fig. 7*A*). Both chimeras consist of a hHCN4 backbone, *i.e.* the whole sequence from START to amino acid 602 (for numbering see Supplemental Fig. S3, hHCN4 sequence), is derived from hHCN4. In chimera h4**CNBD/C**h3, the CNBD and the C-terminal sequence after the CNBD (*i.e.* amino acids 603-STOP) is derived from hHCN3, whereas in chimera h4**CNBD**h3, only the CNBD sequence (*i.e.* amino acids 603–721) is derived from hHCN3. The rest of the C terminus is derived from hHCN4. The exchange of only the CNBD resulted in a functional, HCN4-like channel that is modulated by cAMP (Fig. 7, *B* and C). The voltage-dependent activation curve is shifted by 17.8 ± 5.1 mV toward more positive potentials, which is only slightly less than the shift observed for the wild type hHCN4 (Fig. 6*B*). Acceleration of activation, calculated from the time constants of activation, is about 2.8-fold (Fig. 7*C*). This suggests that the CNBD of hHCN3 is capable of binding cyclic nucleotides despite the lack of modulation of the wild type hHCN3 channel by cAMP/cGMP. cAMP modulation, however, is no longer observed with the mutant channel h4**CNBD/C**h3, which has in addition to the CNBD the remarkable short C terminus of hHCN3. Strikingly, the voltage-dependent activation curve is at already more positive potentials, with a $V_{1/2}$ of −82.7 ± 2.3, than the one of hHCN4. In this

respect, this chimera resembles the hHCN3 wild type channel (compare with Fig. 4/TABLE ONE).

DISCUSSION

We were now able to clone and functionally express the human HCN3 channel in HEK293 cells efficiently enough to characterize this channel. The selection of stable cell lines for each of the human HCN channels allowed us to compare all four known hHCN channels with one another.

The human HCN3 channel proved to be a fully functional, hyperpolarization-activated cation channel having activation kinetics, voltage dependence, and ion selectivity as well as cesium and ZD7288 sensitivity within the range of the other HCN channels. As a striking difference to the other hHCNs, however, hHCN3 channels were not modulated by intracellular cAMP. Direct modulation of the activation kinetics by cAMP is a remarkable feature of the other three HCN channels (4–9). The mechanism of the cAMP modulation has been partially elucidated (12). HCN channels possess a cyclic nucleotide binding domain, located in the intracellular C terminus. The C terminus inhibits activation of the channel by an as yet unknown interaction with the core region. Upon binding of cAMP, this inhibition is released, resulting in less energy demand for channel activation, leading to faster activation and a shift of the activation to more positive activation potentials (12). cAMP-dependent modulation is best observed with hHCN2 and hHCN4, whereas hHCN1 is modulated only moderately. It has to be pointed out that the voltage-dependent activation curve of hHCN1 is already at >20 mV more positive potentials than that of hHCN2/4 in the absence of cAMP, indicating that the inhibition by the C terminus is much less in the first place, and thus, release of inhibition has a less pronounced effect. The activation curve of hHCN3 is close to that of hHCN1 channels, suggesting that the inhibition by the C terminus is weak. Interestingly, $V_{½}$ and τ_1 values of the hHCN3 channels are almost identical with those for the cAMP-modulated hHCN4 channel, supporting the notion that the C terminus of hHCN3 channels has a weak control on channel activation.

The reason for the missing cAMP response of hHCN3 channels is unknown. There are single amino acid differences scattered throughout the core region of the HCN channels. The significance of these differences is not known, but they do not seem to be located in relevant sections. For example, the intracellular linker between S4 and S5, shown to be important for pH-dependent modulation (25), and the voltage-dependent gating (26) of the HCN2 channel are identical between the four human HCN channels. Apart from single amino acid differences, there is an insertion in the S3-S4 linker of hHCN3 compared with all other HCNs. Because this linker has also been associated with the gating of HCN channels (27), it could be involved in the observed missing cAMP response even though it is not obvious how an extracellularly located linker could affect cAMP modulation. The CNBD of hHCN3 itself seems to be intact, making binding of cAMP possible. The amino acids identified by Zagotta *et al.* (14) that interact with cAMP in the CNBD of HCN2 are all present. The conservatively exchanged amino acids I455V and I456V were found not to be essential for cAMP binding (14), although they contributed to the CNBD binding pocket in other proteins (15). This proposed integrity of the CNBD of hHCN3 is supported by our mutated hHCN4 channel, in which the whole CNBD was exchanged for the CNBD of hHCN3. This mutant channel is very well modulated by cAMP. Distal of the CNBD, hHCN3 has the shortest C terminus of all HCNs. This may lead to less basic inhibition. This idea is supported by our chimeric hHCN4 channel, which possesses the CNBD and C-terminal region downstream of the CNBD from hHCN3. This channel is also shifted to more positive potentials and is not further modulated by cAMP. The short, "improper" C terminus does not seem to be able to control channel activation. Like the distal C termini, the N termini of all HCNs differ significantly from one another. Sequences with defined functions, however, such as the part identified to be important for the assembly of four HCN monomers to form functional channels (28), are again conserved in hHCN3. Thus, it is possible that in native tissues hHCN3 forms heterotetrameric HCN channels, with the other HCN subtype(s) contributing the cAMP sensitivity.

Considering the basic properties, hHCN3 channels will fulfill the physiological role of HCN channels, which is the stabilizing effect on the resting membrane potential of cells by tonic contribution of an inward current. Even the contribution to neuronal pacemaker potentials, which requires the concerted action of many ion channels including adaptive ion flow through HCN channels, does not depend as such on cAMP modulation. cAMP-mediated modulation of the current, however, greatly enlarges the functional spectrum of HCN channels. Thus, the challenge remains to unravel the physiological role of HCN3 in brain.

Acknowledgments—We thank Anke Weber for some excellent electrophysiological recordings and Andreas Ludwig for discussions. Specific antibody against HCN3 was kindly provided by Dr. Robert Mader, Department Pharmazie - Zentrum für Pharmaforschung, Ludwig-Maximilians-Universität München, Butenandtstrasse 5-13, 81377 München, Germany. Technical assistance from Anna Thomer is highly appreciated.

REFERENCES

1. Robinson, R., and Siegelbaum, S. (2003) *Annu. Rev. Physiol.* **65,** 453–480
2. Pape, H.-C. (1996) *Annu. Rev. Physiol.* **58,** 299–327
3. Lüthi, A., and McCormick, D. (1998) *Neuron* **21,** 9–12
4. Ludwig, A., Budde, T., Stieber, J., Moosmang, S., Wahl, C., Holthoff, K., Langebartels, A., Wotjak, C., Munsch, T., Zong, X., Feil, S., Feil, R., Lancel, M., Chien, K.R., Konnerth, A., Pape, H.-C., Biel, M., and Hofmann, F. (2003) *EMBO J.* **22,** 216–224
5. Santoro, B., Liu, D. T., Yao, H., Bartsch, D., Kandel, E. R., Siegelbaum, S. A., and Tibbs, G. R. (1998) *Cell* **93,** 717–729
6. Ishii, T. M., Takano, M., Xie, L.-H., Noma, A., and Ohmori, H. (1999) *J. Biol. Chem.* **274,** 12835–12839
7. Ludwig, A., Zong, X., Jeglitsch, M., Hofmann, F., and Biel, M. (1998) *Nature* **393,** 587–591
8. Moosmang, S., Stieber, J., Zong, X., Biel, M., Hofmann, F., and Ludwig, L. (2001) *Eur. J. Biochem.* **268,** 1646–1652
9. Ludwig, A., Zong, X., Stieber, J., Hullin, R., Hofmann, F., and Biel, M. (1999) *EMBO J.* **18,** 2323–2329
10. Qu, J., Altomare, C., Bucchi, A, DiFrancesco, D., and Robinson, R. (2002) *Eur. J. Physiol.* **444,** 597–601
11. Wang, J., Chen, S., Nolan, M., and Siegelbaum, S. (2002) *Neuron* **36,** 451–561
12. Wainger, B., DeGennaro, M., Santoro, B., Siegelbaum, S., and Tibbs, G. (2001) *Nature* **411,** 805–810
13. Stieber, J., Thomer, A., Much, B., Schneider, A., Biel, M., and Hofmann, F. (2003) *J. Biol. Chem.* **278,** 33672–33680
14. Zagotta, W., Olivier, N., Black, K., Young, E., Olson, R., and Gouaux, E. (2003) *Nature* **425,** 200–205
15. Berman, H., Eyck, L., Goodsell, D., Haste, N., Kornev, A., and Taylor, S. (2005) *Proc. Natl. Acad. Sci. U. S. A.* **102,** 45–50
16. Mistrik, P., Mader, R., Michalakis, S., Weidinger, M., Pfeifer, A., and Biel, M. (2005) *J. Biol. Chem.* **280,** 27056–27061
17. Ludwig, A, Zong, X, Hofmann, F., and Biel, M. (1999) *Cell. Physiol. Biochem.* **9,** 179–186
18. Stieber, J., Herrmann, S., Feil, S., Löster, J., Feil, R., Biel M., Hofmann, F., and Ludwig, A. (2003) *Proc. Natl. Acad. Sci. U. S. A.* **100,** 15235–15240
19. Shi, S., Wymore, R., Yu, H., Wu, J., Wymore, R.T., Pan, Z., Robinson, R., Dixon, J., McKinnon, D., and Cohen, I. (1999) *Circ. Res.* **85,** e1–e6
20. Moroni, A., Gorza, L., Beltrame, M., Gravante, B., Vaccari, T., Bianchi, M., Altomare, C., Longhi, R., Heurteaux, C., Vitadello, M., Malgaroli, A., and DiFrancesco, D. (2001) *J. Biol. Chem.* **276,** 29233–29241

21. DiFrancesco, D., Ferroni, A., Mazzanti, M., and Tromba, C. (1986) *J. Physiol.* (*Lond.*) **377,** 61–88
22. Macri, V., and Accili, A. (2004) *J. Biol. Chem.* **279,** 16832–16846
23. BoSmith, R., Briggs, I., and Sturgess, N.C. (1993) *Br. J. Pharmacol.* **353,** 64–72
24. Shin, K., Rothberg, B., and Yellen, G. (2001) *J. Gen. Physiol.* **117,** 91–101
25. Zong, X., Stieber, J., Ludwig, A., Hofmann, F., and Biel, M. (2001) *J. Biol. Chem.* **276,** 6313–6319
26. Chen, J., Mitcheson, J., Tristani-Firouzi, M., Lin, M., and Sanguinetti, M. (2001) *Proc. Natl. Acad. Sci. U. S. A.* **98,** 11277–11282
27. Tsang, S., Lesso, H., and Li, R. (2004) *J. Biol. Chem.* **279,** 43752–43759
28. Tran, N., Proenza, C., Macri, V., Petigara, F., Sloan, E., Samler, S., and Accili, E. (2002) *J. Biol. Chem.* **277,** 43588–43592